

## Influence of hot deformation and composition on microstructure development of magnesium-stannide alloys

Divija Pandel\*<sup>1</sup> and Malay K. Banerjee<sup>2</sup>

<sup>1</sup> Department of Materials Research Centre, MNIT, Jaipur 302017, India

<sup>2</sup> Department of Metallurgical and Material Engineering, MNIT, Jaipur 302017, India

(Received May 26, 2018, Revised May 21, 2020, Accepted September 12, 2020)

**Abstract.** The microstructural evolution of different compositions of Mg-Sn alloys (30%Sn-70%Mg, 40%Sn-60%Mg and 50%Sn-50%Mg) is studied at first to understand the changes observed with change in tin content and deformation conditions. The Mg<sub>2</sub>Sn phase increases with increase in tin content and a significant substructure development is found in 50%Sn-50%Mg alloy. The above observation led to further deformation studies on Mg<sub>2</sub>Sn based thermoelectric materials with higher tin percentage. The microstructure in terms of Electron backscatter diffraction (EBSD) measurements is studied in detail followed by the determination of thermoelectric properties i.e., Seebeck coefficient and electrical conductivity for both as cast and extruded Mg<sub>(2+x)</sub>Sn-Ag alloys. The electrical conductivity of the extruded Mg<sub>(2+x)</sub>Sn-3wt%Ag {x = 1} alloy was found to be more than its as cast counterpart while the Seebeck coefficient values remained almost the same.

**Keywords:** thermoelectric materials; magnesium tin alloys; microstructure; deformation; annealing

### 1. Introduction

In recent times, magnesium based alloys are becoming a preferred choice for various industrial, automotive, biomedical and aerospace applications (Mezbahul-Islam *et al.* 2014). Magnesium besides being light weight, environment friendly and cheap has excellent dimensional stability, high strength and thermal properties (Mark). These advantages have constantly led Magnesium based alloys to be researched for new possibilities in the field of science and innovation.

Implementing sustainable sources of energy is the need of hour and so a huge boost to the on-going studies on thermoelectric materials is seen in some current years. Thermoelectric materials are the one which convert thermal energy into electrical energy (Seebeck effect) and vice versa (Peltier effect). These solid-state devices having no moving parts operate on a simple principle and are highly reliable. Though they have been used widely in many power generation and cooling applications, their low thermoelectric efficiency (denoted by thermoelectric figure of merit ZT) makes them less competent for cost effective commercial uses. Thermoelectric figure of merit (ZT) is a dimensionless quantity given by the expression:

---

\*Corresponding author, Ph.D. Scholar, E-mail: 2017rmr9001@mnit.ac.in

<sup>a</sup> Professor, E-mail: mkbanerjee.meta@mnit.ac.in

$$ZT = 2^2 \sigma T / \kappa \quad (1)$$

where,  $S$  (V/K) is the Seebeck coefficient,  $\sigma$  ( $\Omega^{-1}\text{m}^{-1}$ ) is the electrical conductivity,  $\kappa$  (W/m.K) is the thermal conductivity of TE material and  $T$  (K) is the absolute temperature (Shakouri 2011, Elsheik *et al.* 2014, An *et al.* 2012b, Zheng 2008).

A good thermoelectric material should have high Seebeck coefficient, high electrical conductivity and low thermal conductivity. Doping the material with a suitable dopant can enlarge the electrical conductivity as increased density of charge carriers would result in higher carrier concentration subsequently leading to increased electrical conductivity (Snyder and Toberer 2008). The electrical conductivity of a thermoelectric material is given by the following equation:

$$\sigma = ne\mu \quad (2)$$

where  $n$  is the density of charge carriers,  $e$  is the charge of unit carrier and  $\mu$  is the mobility of charge carriers (Chao *et al.* 2014). However, doping also leads to increased scattering between dopants and charge carriers which might affect the mobility of the charge carriers leading to lower electrical conductivity values (Snyder and Toberer, 2008). Apart from electrical conductivity, another intrinsic property of the material is Seebeck coefficient which is expressed as:

$$S = V / (T_h - T_c) \quad (3)$$

where  $S$  is the Seebeck coefficient in (V/K) and  $V$  is the open circuit voltage in volts.  $T_h$  and  $T_c$  are the temperatures of hot and cold sides, respectively. As mentioned above electrical conductivity and Seebeck coefficient both need to be high for a good thermoelectric material. Chemical composition of semiconductors and doping level influence both of these above stated quantities. High thermopower could only be achieved if the excitation of minority charge carriers at high temperatures has a reduced effect on the majority charge carriers. For good thermoelectric performance, thermopower values should be of the order of 150-250  $\mu\text{V/K}$  (Bashir *et al.* 2014, Bux *et al.* 2010, Minnich *et al.* 2009, Tritt and Subramanian 2006). Another important thermoelectric property is the thermal conductivity which should be low for a better thermoelectric performance. For reducing the thermal conductivity in thermoelectric materials, the lattice component of thermal conductivity needs to be focussed upon. Phonon scattering lowers the lattice thermal conductivity of a material. This could be achieved by using complex structure materials (with heavy atomic weight), point defects, nanograin structures, grain boundaries (Fedorov *et al.* 2006, Bashir *et al.* 2014, Bux *et al.* 2010, Tritt 2004, Lu *et al.* 2014, Thiagarajan *et al.* 2010).

The most commercially used thermoelectric materials are the solid solutions of  $\text{Bi}_2\text{Te}_3$ ,  $\text{Sb}_2\text{Te}_3$  and  $\text{PbTe}$  and  $\text{SiGe}$  alloys (Biswas *et al.* 2012, Tritt 2002, Snyder and Toberer 2008). These alloy compositions are generally quite expensive and also not environment friendly. Magnesium based thermoelectric alloys i.e.,  $\text{Mg}_2\text{X}$  ( $X = \text{Si}, \text{Sn}, \text{Ge}$ ) can achieve higher  $ZT$  values besides being cheap and keeping the environment clean (Jiang *et al.* 2013). They are emerging as the best class of thermoelectrics to be used in the mid temperature range ( $\sim 125^\circ\text{-}525^\circ\text{C}$ ) (Viennois *et al.* 2012, Fedorov *et al.* 2006). It has been reported by Fedorov *et al.* 2006, that  $\text{Mg}_2\text{Si-Mg}_2\text{Sn}$  system show favourable results in the above stated temperature range due to its well-defined combination of band structure and transport properties.

Deformation brings various changes in the microstructure of a material; affecting its grain size, sub-grain size and dislocation density (Humphreys and Hatherly 2004). It is also capable of altering

the thermoelectric and mechanical properties of a material as the grain size, grain orientation (texture) and carrier concentration vary with deformation (Lee *et al.* 2006, Kitagawa *et al.* 2010). Deformation of magnesium alloys at high temperatures can be done by methods like rolling, extrusion and forging. This helps in enhancing the workability of these alloys and the final grain size and the properties of a material are transformed to a great extent. The process that controls the grain size and is quite important during deformation of magnesium alloys is dynamic recrystallization (DRX) (Beer and Barnett 2007, Ion *et al.* 1982). This phenomenon usually occurs at elevated temperature resulting in a refined microstructure, reduced flow stress and improved hot plasticity (Humphreys and Hatherly 2004, Lee *et al.* 2006, Kitagawa *et al.* 2010, Xu *et al.* 2015, Beer and Barnett 2007, Ion *et al.* 1982, Chen *et al.* 2010). It is also shown that electrical properties are enhanced using the hot deformation process. With increase in highly preferred orientations, higher electrical conductivity is observed. The degree of texture is majorly determined by grain sizes and composition of an alloy which can be altered using hot deformation (Hu *et al.* 2012).

For widespread commercial applicability of thermoelectric materials, high thermoelectric performance along with better mechanical stability is required. Heat treatment is a major process that can improve the structure and physical properties of a material. Annealing, one of the mostly used heat treatment techniques helps obtaining refined grain structures in alloys by relieving internal stresses inside the material (Lee *et al.* 2006, 2014). Deformation increases the free energy of the system by introducing various defects and interfaces. The defects can be removed by annealing and the thermal stability could be enhanced by bringing it into a lower energy configuration. Annealing has majorly three important stages; recovery, recrystallization and grain growth (Chen *et al.* 2010).

The substructure of an alloy has a great impact on the thermoelectric properties which could be altered through deforming the alloys. Bipolar thermal conductivity ( $\kappa_b$ ) is a signature of electron hole coupling. Bipolar thermal transport is a conductivity limiting phenomenon and hence its reduction is favourable for thermoelectric properties. Nanostructure reduces bipolar thermal conductivity ( $\kappa_b$ ). Mobility ratio of electron and hole determines bipolar thermal conductivity in intrinsic semiconductor; for heavily doped semiconductor mobility ratio cannot describe  $\kappa_b$  rather for *p*-type heavily doped semiconductor, significant value of  $\kappa_b$  can be noted even at higher mobility ratio. It is determined by the minority carrier partial conductivity in extrinsic semiconductor. Preferential scattering of minority carrier reduces  $\kappa_b$ ; its significant reduction is possible nanostructuring that leads to scattering of minority carrier. Bipolar thermal conductivity is controlled by minority carrier partial conductivity; manipulating  $\kappa_b$  via preferential minority carrier scattering to tune thermoelectric properties favourably (Wang *et al.* 2015). Thus, introducing more scattering centres by way introducing crystal defect seems to be effective. Hence, attempt is made to create substructure by way deformation by extrusion. The substructures may act as effective means to scatter minority charge carrier thereby improving Seebeck coefficient.

The outcome of the effect of deformation enhancing the overall figure of merit of different thermoelectric materials especially  $\text{Bi}_2\text{Te}_3$  based materials has often been reported but there is a gap in understanding its effect on the substructure of the  $\text{Mg}_2\text{Sn}$  alloy. The role of structural stability of these alloys at high temperatures also needs to be studied. Since the preliminary investigation into the substructure studies of magnesium based thermoelectric alloys is lacking; for this reason this study is done, which explores the substructure development and subsequent changes in thermoelectric properties of  $\text{Mg}_2\text{Sn}$  based alloys during hot deformation.  $\text{Mg}_2\text{Sn}$  alloy has an added advantage of having highest hole to electron mobility ratio which makes it a desirable alloy for *p*-type doping. Compared to *n*-type doped Magnesium based thermoelectric alloys, the performance of *p*-type doped systems is clearly subsidiary in many aspects. So for this reason, research in this

field regards special attention. An *et al.* (2012a), Chen and Savvides (2009) and Kim *et al.* (2014) have all integrated silver (Ag) as the *p*-type dopant for the Mg<sub>2</sub>Sn thermoelectric materials in their work. It is observed that doping the system with silver resulted in much better power factor values as compared to the undoped Mg<sub>2</sub>Sn alloy. Choi *et al.* (2012), in their study compared the thermoelectric performance other *p*-type dopants like Nickel (Ni), Copper (Cu), Zinc (Zn) and Indium (In) with Ag on the Mg<sub>2</sub>Sn system. As compared to silver, the carrier concentration of the other dopants was very less leading to very low electrical conductivity values. As a result, the silver doped alloy had the highest power factor and therefore thermoelectric performance. In this study we first examine the effect of extrusion on the microstructure of magnesium stannide alloys. Later the high tin content Mg<sub>2</sub>Sn thermoelectric alloys are prepared and the thermoelectric performance of the undoped and silver doped Mg<sub>2</sub>Sn alloys is studied in detail with change in the microstructure and extrusion effects.

## 2. Experimental procedure

To study the effect of deformation on the microstructure of magnesium stannide (Mg-Sn) alloys, three compositions of Mg-Sn alloys were prepared, the nominal compositions of which by weight percent are: 30%Sn-70%Mg, 40%Sn-60%Mg and 50%Sn-50%Mg. These alloys were then extruded using a laboratory extrusion rig at 500°C and 0.1 mm/s ram speed. Cast billets of 30mm were extruded to 10 mm diameter using an extrusion ratio of 9. After studying the microstructure of these alloys, high tin content Mg<sub>2</sub>Sn based alloys were prepared using the radio frequency (RF) induction melting process. These cast ingots were provided by CSIRO Australia. Composition of these alloys are Mg<sub>(2+x)</sub>Sn {x = 0; (Mg wt.% = 29.06, Sn wt.% = 70.94)} and Mg<sub>(2+x)</sub>Sn-Ag {x = 1; (Mg wt.% = 37.95, Sn wt.% = 61.77, Ag wt.% = 0.28)}. These alloys were then extruded at 400°C and cast billets of 30 mm diameter were extruded in to 15 mm.

Microstructural investigation was carried out using EBSD (Electron backscatter diffraction) by SEM Zeiss Leo 1530 and Bruker Nova Nanosem 450. The collected data is further processed using Project Manager software module. Metallographic process of sample preparation included cold mounting of specimen in epoxy resin followed by grounding it on 1200 grit abrasive paper and then polishing with 6 and 3 μm. Colloidal silica solution was used to polish the samples in the end.

## 3. Results

### 3.1 Microstructural development

In view of the fact that controlled hot deformation of alloys envisages structural refining, it appears prudent to study the influence of extrusion on evolution of microstructure in magnesium stannide (Mg-Sn) alloys that is studied with the aid of Electron backscatter diffraction. The phase maps of 30%Sn-70%Mg, 40%Sn-60%Mg and 50%Sn-50%Mg respectively along the extrusion direction (ED vertical) are shown in Fig. 1. It is apparent that the microstructure consists of two phases Magnesium (hexagonal close-packed-hcp), represented by maroon colour and Mg<sub>2</sub>Sn (cubic) represented by green colour. With increase in the tin content, the phase fraction of Mg<sub>2</sub>Sn grains increased from 19.27% for 30%Sn-70%Mg to its highest at 49.9% for 50%Sn-50%Mg alloy. The misorientations plotted between the neighbouring pixels give the grain boundaries. The

misorientations greater than 2° and less than 15° conform to the sub-grain or low angle grain boundaries (coloured red) and the misorientations greater than 15° are shown by high angle grain boundaries (coloured black). Due to extrusion, the Mg<sub>2</sub>Sn grains are elongated along the extrusion direction, while the grains of Magnesium phase remain equiaxed. This indicates that Mg<sub>2</sub>Sn is only partially recrystallized. The existence of a deformation substructure within the larger grains is indicated by the presence of red boundaries (2°). Partial static recrystallization/ recovery is evidenced in some grains in which low angle grain boundaries are absent. The recrystallization temperature of Mg<sub>2</sub>Sn is higher than magnesium and the drive force for recrystallization available to overall system (magnesium plus magnesium stannide) is spent for recrystallization of magnesium of hcp structure rather than that for zintl phase Mg<sub>2</sub>Sn. The grain and sub-grain sizes of the Mg and Mg<sub>2</sub>Sn phases are calculated using mean lineal intercept method using hkl software. The grain size values are furnished in Table 1.

Table 1 Calculated grain size calculation of Mg-Sn alloys of different compositions (Extrusion direction vertical)

	30%Sn-70%Mg		40%Sn-60%Mg		50%Sn-50%Mg	
GB cut off angle	2°	15°	2°	15°	2°	15°
Mg GS	3.7 μm	4.5 μm	3.04 μm	4.1 μm	2.7 μm	3.2 μm
Mg <sub>2</sub> Sn GS	1.5 μm	1.6 μm	2.5 μm	2.9 μm	2.2 μm	3.1 μm

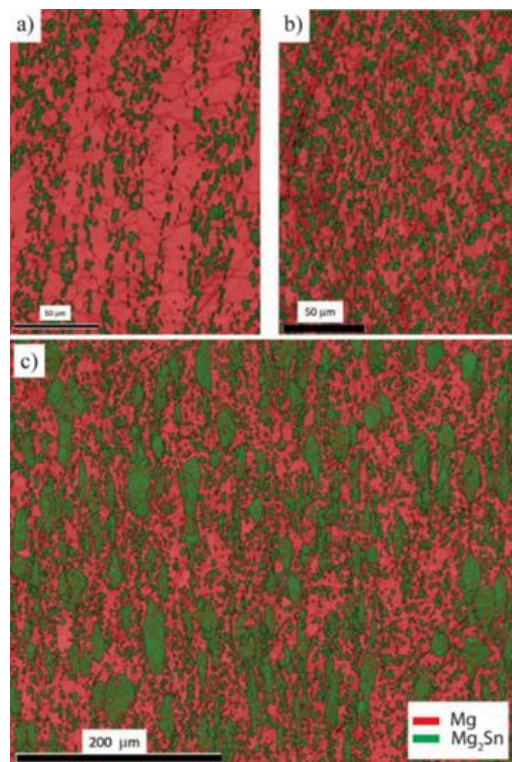


Fig. 1 Phase Maps of (a) 30%Sn-70%Mg; (b) 40%Sn-60%Mg; and (c) 50%Sn-50%Mg (extrusion direction vertical)

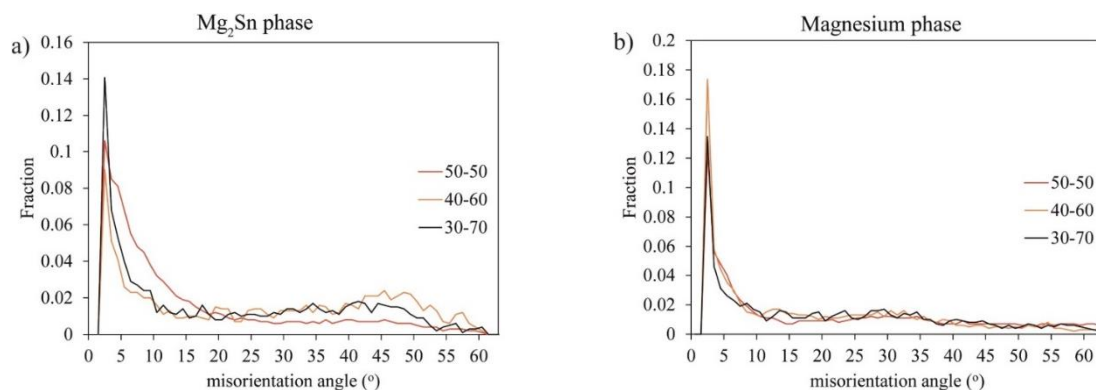


Fig. 2 Misorientation distribution of (a)  $Mg_2Sn$  phase; and (b) Magnesium phase of Mg-Sn alloys (along extrusion direction)

The misorientation distribution plots for the three Mg-Sn alloys are shown in Fig. 2. The sub-grain evolution in Magnesium and  $Mg_2Sn$  phase could be assessed using these plots. For the  $Mg_2Sn$  phase, a relatively high fraction of low angle grain boundaries with misorientation about  $2^\circ$  is observed in all the alloys. The second peak at about  $45^\circ$  correlates to the high angle grain boundaries. A remarkable increase in the misorientations in the range of  $5-15^\circ$  is observed in the  $Mg_2Sn$  phase of the 50%Sn-50%Mg alloy. This is due to the development of a sub-grain structure which possibly relates to the high fraction of interface boundary resulting in detaining of the generation of deformation induced high angle grain boundaries. Such observation in higher tin alloy (hence higher volume fraction of  $Mg_2Sn$ ) is the manifestation of accumulation of densely populated dislocations at the boundaries. In such a two-phase material, magnesium is the major phase in first two alloys whereas in 50%Sn-50%Mg composition the two phases are seen to be of equal proportion. In normal cases the deforming load in biphasic material is shared between the two phases and the share is more for the softer phase. Therefore, magnesium being a softer and major phase shared majority of extrusion load and having experienced a higher amount of deformation could undergo complete recrystallization at the extrusion temperature. In contrast, for the 50%Sn-50%Mg alloy the constituents (Mg and  $Mg_2Sn$ ) are equiproportionate and so the deformation load shared by  $Mg_2Sn$  had led to a little higher amount of deformation. It is known that recrystallization of alloys is possible only if the amount of deformation is high enough to exceed a critical value commensurate with the temperature of working. From the experimental observation it appears that even with increased amount of extrusion load sharing, the deformation of  $Mg_2Sn$  has not been high enough to give rise to the formation of strain free grains (that is completely recrystallized grains) characterised by large angle grain boundaries. Under such situation recovery is inevitable and the dislocations generated during hot deformation have accumulated at the sub grain boundaries thereby increasing the angle of misorientation across the sub grain boundaries. This observation has enticed the authors to probe into the evolution of sub-grain boundaries in higher tin content alloys i.e.,  $Mg_{(2+x)}Sn$   $\{x = 0\}$  and  $Mg_{(2+x)}Sn$ -3wt%Ag  $\{x = 1\}$ .

The Electron backscatter diffraction (EBSD) microstructures of extruded  $Mg_{(2+x)}Sn$   $\{x = 0\}$  and  $Mg_{(2+x)}Sn$ -3wt%Ag  $\{x = 1\}$  alloys are shown in Fig. 3. Cubic  $Mg_2Sn$  (light green) and hexagonal crystal-packed Magnesium (HCP) phase (blue) are the two phases observed in the microstructure. In both the maps, most of the space is covered by the  $Mg_2Sn$  phase ( $\sim 97\%$ ) while Magnesium (Mg) phase can only be seen in traces. Since the magnesium phase is only about 3% of the total

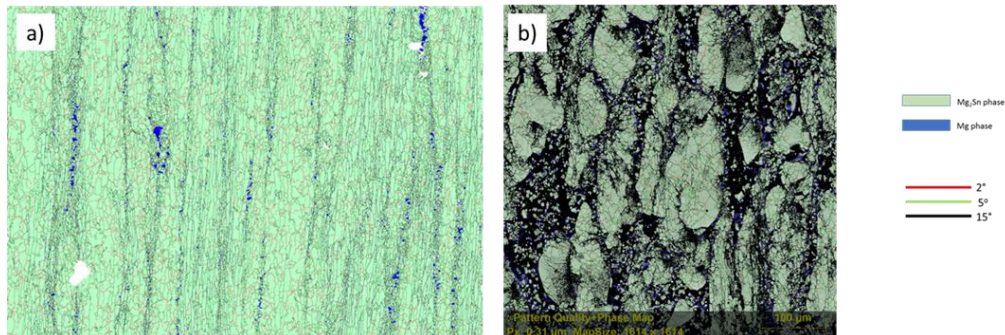


Fig. 3 Phase maps of (a)  $Mg_{(2+x)}Sn$   $\{x = 0\}$ ; and (b)  $Mg_{(2+x)}Sn$ -.3wt%Ag  $\{x = 1\}$  alloys (extrusion direction vertical)

microstructure, it does not provide adequate numbers of grains to employ Electron backscatter diffraction (EBSD) for measurement of the grain sizes and the misorientations of the magnesium phase. For this reason the grain sizes and misorientations of the magnesium phase could not be calculated. The  $2^\circ$  and  $5^\circ$  misorientations are the sub-grain or low angle boundaries while the misorientations in black denote high angle grain boundaries. In the Mg phase of  $Mg_{(2+x)}Sn$   $\{x = 0\}$  alloy, only high angle grain boundaries ( $15^\circ$  misorientations) were noticed while the same could not be confirmed for the  $Mg_{(2+x)}Sn$ -.3wt%Ag  $\{x = 1\}$  alloy because the Mg phase was not properly indexed in this case. On the other hand, a clear substructure ( $2^\circ$  and  $5^\circ$  misorientations) is observed in the  $Mg_2Sn$  phase which supports the idea that the  $Mg_2Sn$  alloys can be adequately deformed to produce deformation substructure which may exert a positive influence of the thermoelectric properties of these alloys and thus enhancement of thermoelectric efficiency. Further processing of this alloy in terms of evaluation of grain sizes, texture and heat treatment analysis would be carried out in future and is not in the scope of this paper. In the upcoming sections, a comparison of thermoelectric properties (Seebeck coefficient and electrical conductivity) is attempted as a part of the deformation study on the as cast and extruded  $Mg_{(2+x)}Sn$ -.3wt%Ag  $\{x = 1\}$  alloy.

### 3.2 Texture evolution in Mg-Sn alloys

Inverse pole figures have been plotted to study the evolution of preferred orientation (texture) during extrusion in 30%Sn-70%Mg, 40%Sn-60%Mg and 50%Sn-50%Mg alloys. The inverse pole figures (IPFs) are plotted along the extrusion direction. The inverse pole figures for  $Mg_2Sn$  and Mg phase are shown in Fig. 4. Magnesium phase, in all three alloys exhibited the standard extrusion texture of  $\langle 01-10 \rangle$  and  $\langle -12-10 \rangle$  along extrusion direction. The preferred orientation of grains in  $Mg_2Sn$  phase is towards  $[001]$  direction. The texture strengthened for both Mg and  $Mg_2Sn$  phases with increase in tin content in the alloys.

The evolution of texture has also been studied for  $Mg_2Sn$  phase of  $Mg_{(2+x)}Sn$   $\{x = 0\}$  alloy. It is observed in the instant case (Fig. 5) that the direction of preferred orientation of grains is different from what we observed for the cases of 30%Sn-70%Mg, 40%Sn-60%Mg and 50%Sn-50%Mg alloys. It appears that  $Mg_2Sn$  grains exhibit preferred orientation along the direction that is close to  $\langle 111 \rangle$  direction with a few degrees angular shift. The report on deformation texture of  $Mg_2Sn$  is scarce in the literature; therefore, there is little scope for the authors to authenticate the validity of current observation against a standard deformation texture of hot extruded  $Mg_2Sn$  alloys.  $Mg_2Sn$  is

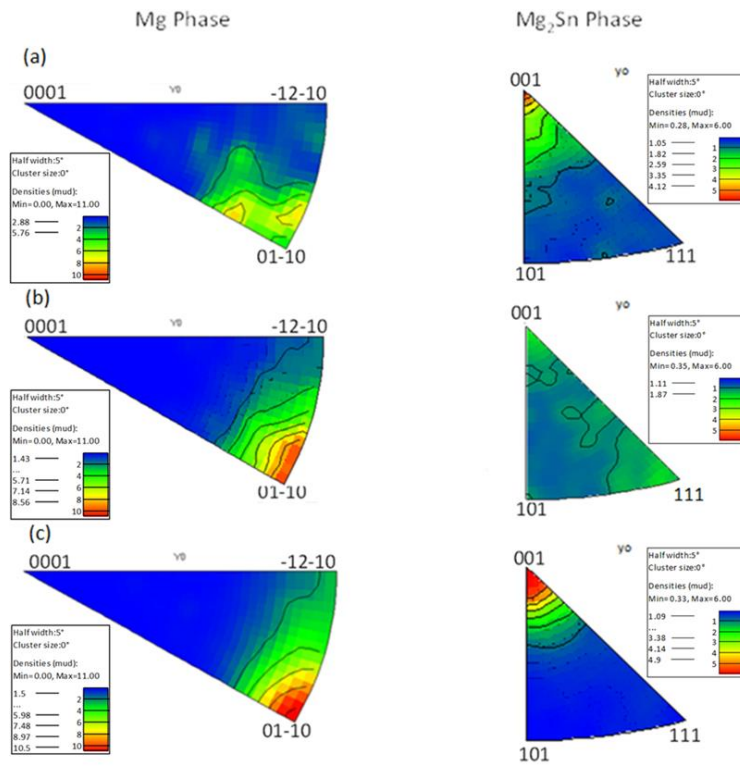


Fig. 4 Inverse pole figures for (a) 30%Sn-70%Mg; and (b) 40%Sn-60%Mg; and (c) 50%Sn-50%Mg (extrusion direction vertical)

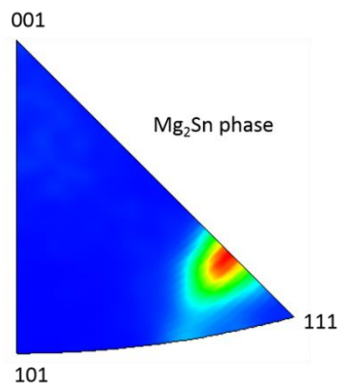


Fig. 5 Inverse pole figure of  $Mg_{(2+x)}Sn$   $\{x = 0\}$  (extrusion direction vertical)

Fluorite structured and crystallizes in the cubic Fm-3m space group. Again, it is reported elsewhere that slip deformation in cubic crystals promote a grain orientation along [111]; quite often a common deformation texture of cubic crystal is characterized by copper  $\{112\} \langle 111 \rangle$ . In the unit cell fluorite structured  $Mg_2Sn$ , the four tin atoms arrange in fcc manner whereas the eight magnesium atoms are organized in the tetrahedral form. In the light of above information, it may be fairly presumed that

the present observation of preferred orientation of  $Mg_2Sn$  along [111] is logically consistent and is harmonious to previous observation of deformation texture of common cubic crystals (Chapellier *et al.* 1990 and Ray and Jonas 1990).

### 3.3 Heat treatment analysis of extruded Mg-Sn alloys

The extruded Mg-Sn samples were annealed at two different temperatures; 350°C and 400°C for different annealing times. The Electron backscatter diffraction map of 50%Sn-50%Mg sample annealed at 400°C for 6 hours is shown in Fig. 6. The  $Mg_2Sn$  grains are coloured green while the Magnesium grains are coloured red. A bimodal distribution of grains in the  $Mg_2Sn$  phase appears because of extrusion. As previously discussed, the sharing of extrusion load has not been adequate to insure complete recrystallization of  $Mg_2Sn$  phase in an otherwise constrained surroundings of equal proportion of elemental magnesium, only partial recovery could occur. Thus, partially recovered structure is indicated by the large  $Mg_2Sn$  islands whereas fine  $Mg_2Sn$  grains are subjected to completely recrystallized state. As expected, It can be noticed from the figure that the deformed structure is not completely removed by annealing as low angle grain boundaries (2-15°) are still present in significant amount in the  $Mg_2Sn$  phase of 50%Sn-50%Mg annealed sample. This might be due to the fact that inadequate deformation of  $Mg_2Sn$  in this biphasic material has led to recovery of some grains. Such recovered grains do not undergo subsequent recrystallization owing to the stability of the substructure. Presumably, the presence of recovered grains in the microstructure is supportive to the conjecture that deformed structure is relatively stable. However, the microstructure of the annealed alloys discerns increase in fraction of high angle grain boundaries and as explained earlier, these owe their origin to static recrystallization occurring during the annealing process. The sub-grain size (2° misorientation) of  $Mg_2Sn$  increased from 2.2  $\mu m$  for the extruded alloy to 5.5  $\mu m$  for the annealed alloy. The grain size (for a 15° cut off) in  $Mg_2Sn$  phase, increased from 3.1  $\mu m$  to 7.5  $\mu m$  and from 3.2  $\mu m$  to 5.3  $\mu m$  for the magnesium phase.

The influence of annealing on hardness of the material is shown in Fig. 7 for 30%Sn-70%Mg and 50%Sn-50%Mg samples. The Dura Scan 20, Struers Vickers hardness testing machine was used to conduct Vickers micro hardness measurements. The peak load was set to HV 0.3 (300 g) with an objective lens of 10X and x2 zoom. The dwell time was kept to be 15 sec. The hardness was taken as an average of approximately 20 indents made randomly on the sample. With increase in tin content the hardness of Mg-Sn alloys increases (Liu *et al.* 2007). The same is observed in our

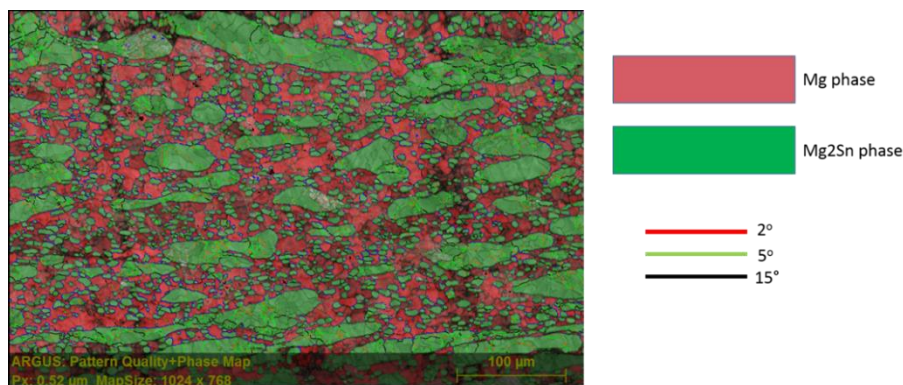


Fig. 6 Phase Map of 50%Sn-50%Mg annealed at 400°C for 6 hours (extrusion direction horizontal)

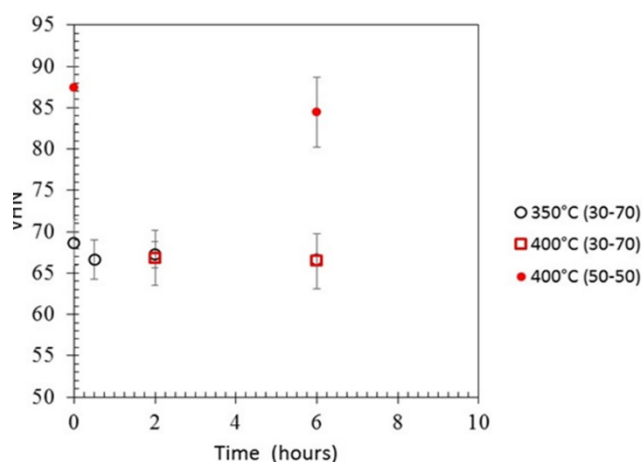


Fig. 7 Hardness values of annealed samples of 30%Sn-70%Mg and 50%Sn-50%Mg composition

experiments; the hardness of Mg-Sn samples increased from 68VHN for 30%Sn-70%Mg to 87VHN for 50%Sn-50%Mg. In agreement with these values, it can be seen from the figure that the hardness of the 50%Sn-50%Mg sample stayed above 30%Sn-70%Mg sample for different annealing times and temperatures. The increase in hardness value with increasing tin content is natural. The measured hardness value of this two-phase material represents the composite strengthening and is given by the weighted average of the hardness values of individual phases. The hardness of metallic magnesium in deformed and annealed state is about 40-45 VHN (Sahoo *et al.* 2015) whereas that for pure Mg<sub>2</sub>Sn phase is around 150-200 VHN. Moreover, the fraction of Mg<sub>2</sub>Sn increases with increasing tin content. Hence, average hardness value is seen to have increased. Although, it is expected that annealing of deformed alloy should lead to some softening due to recrystallization, there has not been any such evidence of reduction in hardness value due to annealing at 400°C for 6 hours. Further experiments are needed to understand such apparently anomalous behaviour. Since no substantial difference is observed in the extruded and annealed alloy, the higher tin content Mg<sub>2</sub>Sn alloys did not undergo any annealing process.

### 3.4 Thermoelectric measurements

#### 3.4.1 Seebeck coefficient and electrical conductivity

Seebeck coefficient is a property dependent on the material's electronic structure and is given by the amount of voltage generated per unit temperature gradient. The Seebeck coefficient sign is positive for P-type semiconductors and is negative for n-type semiconductors that exhibit electron conduction (Bashir *et al.* 2014, Bux *et al.* 2010, Minnich *et al.* 2009). It can be optimized using appropriate chemical composition, heavy doping and band engineering to lead to band convergence. Moreover, high density of states near Fermi level is conducive for enhancement of Seebeck coefficient. Also, the minority charge carriers play a significant role in influencing the values of thermopower. To achieve high thermopower in high temperature applications, the concentration of minority charge carriers needs to be reduced (Bashir *et al.* 2014, Bux *et al.* 2010, Minnich *et al.* 2009, Tritt and Subramanian 2006).

The variation of Seebeck coefficient with respect to temperature change for Mg<sub>(2+x)</sub>Sn-.3wt%Ag

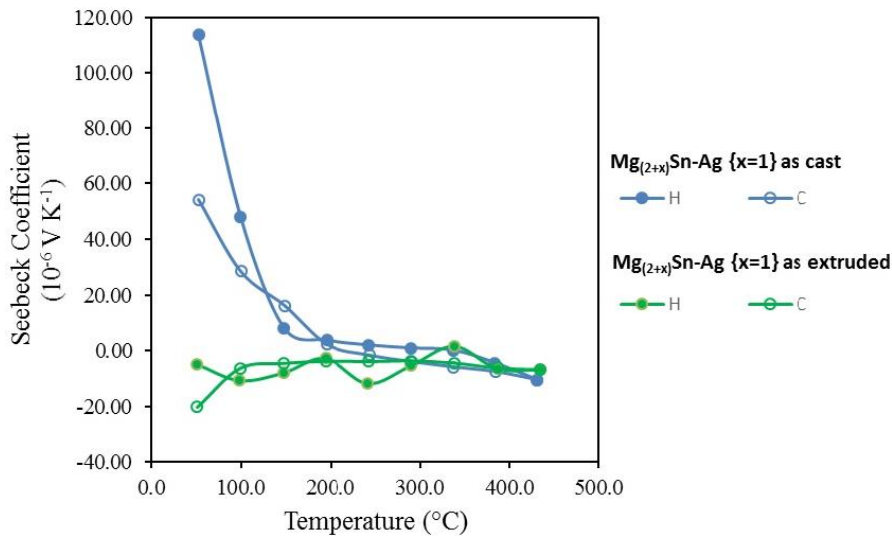


Fig. 8 Variation of Seebeck coefficient for  $Mg_{(2+x)}Sn-.3wt\%Ag \{x = 1\}$  as cast and as extruded alloys as a function of temperature

$\{x = 1\}$  thermoelectric alloy are shown in Fig. 8. The heating cycle (H) is represented by the filled symbols and the unfilled symbols signify cooling (C). From the figure, it can be seen that the as cast alloy curve starts with a larger positive Seebeck coefficient which then decreases with increase in temperature. Negative values for this alloy have been shown at only higher temperatures ( $\sim 384$ - $430^\circ\text{C}$ ) while the Seebeck coefficient values of the extruded alloy are mostly negative except for a point ( $338^\circ\text{C}$ ) where it is positive. It is shown that the Seebeck coefficient values are significantly different below  $200^\circ\text{C}$ , in the two processing conditions but it remains largely unchanged with extrusion for temperatures above  $300^\circ\text{C}$ . It is observed that the Seebeck coefficient values seem to be converging at higher temperatures for both as cast and extruded alloys.

High electrical conductivity can be achieved by increasing the density of charge carriers as electrical conductivity is directly proportional to the latter. This can be done by effectively doping the material with a suitable dopant (Chao *et al.* 2014). As mentioned before, deformation too brings a significant change in the electrical properties of a system. The change in electrical conductivity of  $Mg_{(2+x)}Sn-.3wt\%Ag \{x = 1\}$  as cast and extruded alloys as a function of temperature is shown in Fig. 9. The extruded alloy is represented by green colour and the as cast alloy by blue. The measurements taken in the temperature range are shown for both heating (filled symbol H) and cooling (unfilled symbol C) cycles.

The electrical conductivity is highest at room temperature and it reduces constantly as the temperature increases for both as cast and as extruded alloys. Addition of excess magnesium increases the metallic behaviour of the alloy due to which electrical conductivity reduces with increasing temperature because of increased phonon-electron and electron-electron scattering. The electrical conductivity values of as extruded  $Mg_{(2+x)}Sn-.3wt\%Ag \{x = 1\}$  alloy are higher than the as cast alloy at every given temperature. Some possible defects in as cast alloy like pin holes, micro and nano pores, micro segregation effects increase the incoherent scattering inside the system and thus the electrical resistivity increases. These defects are removed by extruding the alloy at high temperature and thus the as extruded alloy observes lower values of electrical resistivity as locally

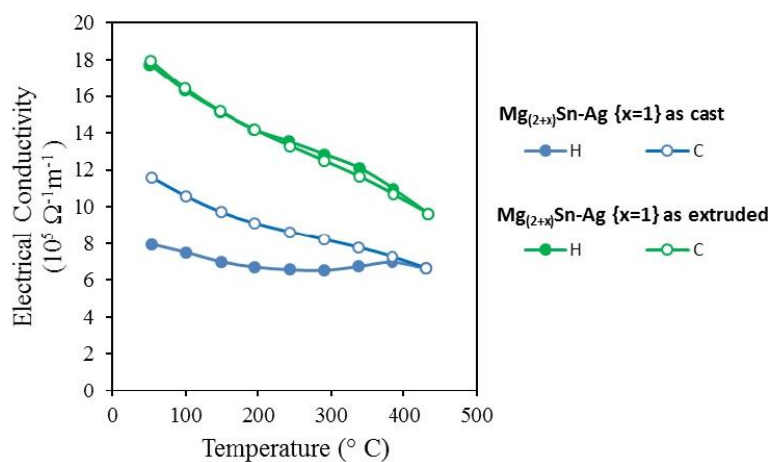


Fig. 9 Variation of electrical conductivity for  $\text{Mg}_{(2+x)}\text{Sn}-.3\text{wt}\% \text{Ag} \{x = 1\}$  as cast and as extruded alloys as a function of temperature

centralized centres for scattering are reduced. The alignment effect of micro constituents might also have influenced the electrical conductivity.

From the foregoing observation it appears that trend of temperature dependence of Seebeck coefficient in extruded alloy is different from that of cast alloy whereas in case of electrical conductivity both extruded and as cast alloy show qualitatively same trend.  $\text{Mg}_2\text{Sn}$  is Fluorite structured and crystallizes in the cubic  $\text{Fm-3m}$  space group.

It is known that  $\text{Mg}_2\text{Sn}$  without doping exhibits  $p$ -type behaviour (hence shows positive Seebeck coefficient) at room temperature and that increasing temperature make Seebeck coefficient convert to  $n$ -type (An *et al.* 2012a). In case of excess magnesium, the transition from  $p$ - to  $n$ -type takes place at comparatively lower temperature due to higher electro positivity. Silver is a strong  $p$ -type dopant and is used to retain the  $p$ -type behaviour over wider temperature range till a higher temperature. It also decreases the lattice thermal conductivity (An *et al.* 2012a). Moreover, the effect of silver doping on the thermoelectric behaviour of  $\text{Mg}_2\text{Sn}$  is dependent on the site specificity of silver atoms in the lattice. When it substitutes Magnesium in the lattice of  $\text{Mg}_2\text{Sn}$ , a rigid-band-like behaviour is observed, otherwise resonant levels are formed. Nevertheless, it leads to furtherance of  $p$ -type conductivity. It was found earlier that the atoms of silver (Ag) normally occupy Mg site (Kim *et al.* 2014). In contrast, the experimental alloy is nonstoichiometric and contains far excess magnesium than what was investigated earlier (An *et al.* 2012a) and therefore, there are reasons to believe that excess magnesium has significantly influenced the Seebeck coefficient. At high temperature, increased lattice vibration might have led to silver atoms occupying tin sites too; in that case resonant levels could have formed and near independency of Seebeck coefficient with temperature had resulted. The observed behaviour of Seebeck coefficient for both as cast and extruded alloy adds credence to our conjecture.

The monotonous decrease in electrical conductivity (Fig. 9) of the alloys suggests that the amount of silver doping done in the present investigation has induced sufficient degeneracy in the  $\text{Mg}_2\text{Sn}$  semiconductor. Owing to crystal structure, the band structure of  $\text{Mg}_2\text{Sn}$  exhibits inherently high level of degeneracy. This  $\text{Mg}_2\text{Sn}$  material exhibits semiconductor to metal transition at high temperature. Moreover,  $\text{Mg}_2\text{Sn}$  is a narrow band gap semiconductor; its band gap is only 0.13 eV and therefore at high temperature it exhibits metallic behaviour and that is why its Seebeck coefficient and hence

power factor is not high. Doping by silver further reduces band gap and aggravates the exposition of intense positive temperature coefficient of resistance. The silver doping brings about degeneracy in  $\text{Mg}_2\text{Sn}$  by enhanced acoustic phonon scattering of charge carrier thereby leading to diminution in mobility of charge carrier (Macario *et al.* 2018 and Santos *et al.* 2018). In line with previous report (Kim *et al.* 2014) silver doping has promoted  $p$ - type conductivity in  $\text{Mg}_2\text{Sn}$ . As stated before, the Zintl phase  $\text{Mg}_2\text{Sn}$  crystallizes in the form of cubic Fm-3m space group. Thus, the two sub-lattices are expected to undergo straining and in case of  $\text{Mg}_2\text{Sn}$ , compressive strain is expected to enhance band valley degeneracy or band convergence; this is known to enhance Seebeck co-efficient (Kim *et al.* 2016). This being the reason for the alloy to exhibit the behaviour of a degenerate semiconductor, the higher conductivity values observed for the extruded alloy over the cast alloy at all temperatures needs further justification. As explained earlier, the detrimental solidification defects are removed during hot working and so the conductivity of extruded alloys is higher.

In a normal case the Seebeck coefficient displays opposite temperature dependence as compared to electrical conductivity. Seebeck coefficient is inversely proportional to carrier concentration which is however independent of temperature until bipolar conduction takes place. The bipolar thermal conductivity,  $\kappa_b$  is determined by the minority charge carrier partial conductivity. Bipolar thermal transport is known to be a conductivity limiting phenomenon (Wang *et al.* 2015). Creating means to scatter minority charge carrier is of great importance to improve thermoelectric property. It is noted from Fig. 9 that the average slope of conductivity vs. temperature curve is steeper in case of extruded alloy. Thus, it is hinted that if there is bipolar conduction, it occurs earlier in extruded alloy than the as cast alloy. As stated earlier, micron level defects could incoherently scatter electrons, which is the minority charge carrier in  $p$ - type material more than extruded alloy. This is in opposition to initial expectation; it seems that the material underwent sufficient recovery and scattering centers like dislocation were not abundant to reduce bipolar conduction. In such a  $p$ -type material, the minority charge carrier is electron; the excess magnesium has enhanced the concentration of minority charge carrier. Thus, in order to effectively reduce  $\kappa_b$  the presence of abundant randomly distributed scattering centers is required. It is found in Fig. 5, that the extruded alloy is textured and EBSD observation also records the presence of higher angle sub grain boundaries; as discussed earlier, this implies that dislocation accumulation is considerably high at sub grain boundaries. Preferred orientation of grains certainly limits the randomness in organization of scattering centers. All these factors have limited the effective scattering centers for minority charge carriers. This accounts for the observation that the Seebeck coefficient in extruded alloy does not vary much with temperature and it is a signature of appreciable bipolar thermal transport which has prohibited in tuning Seebeck coefficient favourably. For the cast alloy too, bipolar conduction effect has been quite appreciable; on the other hand, the similarity in the behaviour of variation of Seebeck Coefficient and conductivity at low temperature regime raises a question if silver doping in  $p$ -type  $\text{Mg}_2\text{Sn}$  has stimulated bipolar conduction in cast sample also at low temperature regime. Again, as stated earlier that the inherent tendency of  $\text{Mg}_2\text{Sn}$  is such as to exhibit the observed trend, therefore, no conclusive remark can be made with the evidence available to the authors under present experimental scheme. However, this will constitute the subject of further study.

$\text{Mg}_2\text{Sn}$  is a double valley semiconductor (Santos *et al.* 2018) and hence its band degeneration is accompanied by band convergence. A good Seebeck coefficient~ 110  $\mu\text{V}/\text{K}$  is related to possible band convergence as is predicted by theoretical calculation due to Johnson and Alam (2018). As reported earlier (Johnson and Alam 2018) band degeneracy enables in obtaining high density of states effective mass ( $m^*_D$ ) which aids in achieving high Seebeck coefficient without harming charge carrier and hence electrical conductivity (Rowe 1995). It is found that the  $p$ -type  $\text{Mg}_2\text{X}$  exhibit

superior thermoelectric performance originating from a large density-of-states effective mass due to the large valley degeneracy of valence bands. It is interesting to note that the maximum Seebeck coefficient is of  $\sim 110 \mu\text{V}/\text{K}$  can be obtained in cast alloy at the room temperature. This is attained at a conductivity level of  $12 \times 10^5 \text{ S/m}$ . Moreover, the lattice thermal conductivity of  $\text{Mg}_2\text{Sn}$  is rather low due to presence of heavy tin atoms which leads to mass disorder scattering of phonons. In addition, doping by silver further reduces the thermal conductivity, because silver atoms replace magnesium in the lattice. Silver being much heavier than magnesium, mass disorder scattering of phonon is further intensified. Taking a stock of available information, it is fair to presume a conductivity of the experimental alloy to be of the order of  $2 \text{ W/mK}$  (Bahk *et al.* 2014). Taking such assumptions it is found that the experimental alloy behaves as a lucrative room temperature thermoelectric material with the capability of yielding a  $zT$  value of 0.25 or above. It is no denying that the results of the current study have lent a new research area to evolve means to harness the potential of defect engineering to improve the thermoelectric efficiency of  $\text{Mg}_2\text{Sn}$ .

#### 4. Conclusions

The current research carries out preliminary investigations to study the microstructures of the extruded  $\text{Mg}$ - $\text{Sn}$  alloys with varying tin concentrations. With increase in tin content, the volume fraction of  $\text{Mg}_2\text{Sn}$  phase increases from 19.7% for 30% $\text{Sn}$ -70% $\text{Mg}$  to 33.6% and 49.9% for 40% $\text{Sn}$ -60% $\text{Mg}$  and 50%-50%  $\text{Mg}$  respectively. The extruded  $\text{Mg}$  alloys containing more than 50%  $\text{Mg}_2\text{Sn}$  have been successfully characterized and further investigations were carried out on these alloys which had  $\text{Mg}_2\text{Sn}$  as their main phase. Significant development of substructure (increased frequency of 2 and 5° misorientations) is seen in the  $\text{Mg}_2\text{Sn}$  phase of the tin rich alloys introduced by extrusion. A very small change in the hardness values is observed upon annealing the  $\text{Mg}$ - $\text{Sn}$  alloys at  $400^\circ\text{C}$  for 6 hours; showing some mechanical stability at high temperatures. The Seebeck coefficient and electrical conductivity of the as cast  $\text{Mg}_2\text{Sn}$  alloy doped with  $\text{Ag}$  is measured and compared with those of the extruded  $\text{Mg}_2\text{Sn}$  alloy. The as cast sample exhibited positive Seebeck coefficient values throughout the temperature range except at higher temperatures while the extruded sample showed n-type behaviour. The values of electrical conductivity and Seebeck coefficient decreased with increase in temperature for both as cast and extruded  $\text{Mg}_2\text{Sn}$  alloys. Overall as compared with the as cast alloy, the Seebeck coefficient remains largely unchanged with extrusion for temperatures above  $300^\circ\text{C}$ . The electrical conductivity, however increases by approximately 1.5 times for the extruded  $\text{Mg}_{(2+x)}\text{Sn}$ - .3wt% $\text{Ag}$   $\{x = 1\}$  alloy. The cast alloy seems to behave as a good room temperature thermoelectric material.

#### References

- An, T.H., Park, C., Soon, W.S., Choi, S.M., Kim, I.H. and Kim, S.U. (2012a), "Enhancement of p-type thermoelectric properties in an  $\text{Mg}_2\text{Sn}$  system", *J. Korean. Phys. Soc.*, **60**, 1717-1723.  
<https://doi.org/10.3938/jkps.60.1717>
- An, T.H., Choi, S.M., Kim, I.H., Kim, S.U., Seo W.S., Kim, J.Y. and Park, C. (2012b), "Thermoelectric properties of a doped  $\text{Mg}_2\text{Sn}$  system", *Renew. Energy*, **42**, 23-27.  
<https://doi.org/10.1016/j.renene.2011.09.030>
- Bahk, J.H., Bian, Z. and Shakouri, A. (2014), "Electron transport modeling and energy filtering for efficient thermoelectric  $\text{Mg}_2\text{Si}_{1-x}\text{Sn}_x$  solid solutions", *Phys. Rev. B*, **89**(7), 075204.

- <https://doi.org/10.1103/PhysRevB.89.075204>
- Bashir, M.B.A., Said, S.M., Sabri, M.F.M., Shnawah, D.A. and Elsheikh, M.H. (2014), "Recent advances on  $Mg_2Si_{1-x}Sn_x$  materials for thermoelectric generation", *Renew. Sustain. Energy Rev.*, **37**, 569-584. <https://doi.org/10.1016/j.rser.2014.05.060>
- Beer, A.G. and Barnett, M.R. (2007), "Microstructural development during hot working of Mg-3Al-1Zn", *Metall. Mater. Trans. A*, **38A**, 1856-1867. <https://doi.org/10.1007/s11661-007-9207-5>
- Biswas, K., He, J., Blum, I.D., Iwu, C., Hogan, T.P., Seidman, D.N., Dravid, V.P. and Kanatzidis, M.G. (2012), "High-performance bulk thermoelectrics with all-scale hierarchical architectures", *Nature*, **489**, 414-418. <https://doi.org/10.1038/nature11439>
- Bux, S.K., Fleurial, J.P. and Kaner, R.B. (2010), "Nanostructured materials for thermoelectric applications", *Chem. Comm.*, **46**(44), 8311-8324. <https://doi.org/10.1039/C0CC02627A>
- Chapellier, P.H., Ray, R.K. and Jonas, J.J. (1990), "Prediction of transformation textures in steels", *Acta Metall. Mater.*, **38**(8), 1475-1490. [https://doi.org/10.1016/0956-7151\(90\)90116-X](https://doi.org/10.1016/0956-7151(90)90116-X)
- Chen, H.Y. and Savvides, N. (2009), "Microstructure and thermoelectric properties of n- and p-type doped  $Mg_2Sn$  compounds prepared by the modified Bridgman method", *J. Electron. Mater.*, **38**, 1056-1060. <https://doi.org/10.1007/s11664-008-0630-1>
- Chen, H.Y., Savvides, N., Dasgupta, T., Stiewe, C. and Mueller, E. (2010), "Electronic and thermal transport properties of  $Mg_2Sn$  crystals containing finely dispersed eutectic structures", *Physica Status Solidi (a)*, **207**, 2523-2531. <https://doi.org/10.1002/pssa.201026119>
- Choi, S.M., An, T.H., Seo, W.S., Park, C., Kim, I.H. and Kim, S.U. (2012), "Doping effects on thermoelectric properties in the  $Mg_2Sn$  system", *J. Electron. Mater.*, **41**, 1071-1076. <https://doi.org/10.1007/s11664-012-1985-x>
- Elsheikh, M.H., Shnawah, D.A., Sabri, M.F.M., Said, S.B.M., Hassan, M.H., Bashir, M.B.A. and Mohamad, M. (2014), "A review on thermoelectric renewable energy: principle parameters that affect their performance", *Renew. Sustain. Energy Rev.*, **30**, 337-355. <https://doi.org/10.1016/j.rser.2013.10.027>
- Fedorov, M.I., Zaitsev, V.K., Gurieva, E.A., Eremin, I.S., Konstantinov, P.P., Samunin, A.Y. and Vedernikov, M.V. (2006), "Highly effective  $Mg_2Si_{1-x}Sn_x$  thermoelectrics", *Phys. Rev. B*, **74**(4), 45207. <https://doi.org/10.1103/PhysRevB.74.045207>
- Han, C., Li, Z. and Dou, S. (2014), "Recent progress in thermoelectric materials", *Chinese Sci. Bull.*, **59**(18), 2073-2091. <https://doi.org/10.1007/s11434-014-0237-2>
- Hu, L., Gao, H., Liu, X., Xie, H., Shen, J., Zhu, T. and Zhao, X. (2012), "Enhancement in thermoelectric performance of bismuth telluride based alloys by multi-scale microstructural effects", *J. Mater. Chem.*, **22**(32), 16484-16490. <https://doi.org/10.1039/C2JM32916F>
- Humphreys, F.J. and Hatherly, M. (2004), *Recrystallization and Related Annealing Phenomenon* (Second Edition).
- Ion, S.E., Humphreys, F.J. and White, S.H. (1982), "Dynamic recrystallization and the development of microstructure during the high temperature deformation of magnesium", *Acta Metall.*, **30**(10), 1909-1919. [https://doi.org/10.1016/0001-6160\(82\)90031-1](https://doi.org/10.1016/0001-6160(82)90031-1)
- Jiang, G., Chen, L., Gao, H., Du, Z., Zhao, X., Tritt, T.M. and Zhu, T. (2013), "Improving p-type thermoelectric performance of  $Mg_2(Ge,Sn)$  compounds via solid solution and Ag doping", *Intermetallics*, **32**, 312-317. <https://doi.org/10.1016/j.intermet.2012.08.002>
- Johnson, D.D. and Alam, A. (2018), "Enhanced thermoelectric performance of  $Mg_2Si_{1-x}Sn_x$  codoped with Bi and Cr", *Phys. Rev B*, **98**(11), 115204. <https://doi.org/10.1103/PhysRevB.98.115204>
- Kim, S., Wiendlocha, B., Jin, H., Tobola, J. and Heremans, J.P. (2014), "Electronic structure and thermoelectric properties of p-type Ag-doped  $Mg_2Sn$  and  $Mg_2Sn_{1-x}Si_x$  ( $x = 0.05, 0.1$ )", *J. Appl. Phys.*, **116**(15), 153706. <https://doi.org/10.1063/1.4898013>
- Kim, C.E., Soon, A. and Stampfl, C. (2016), "Unraveling the origins of conduction band valley degeneracies in  $Mg_2Si_{1-x}Sn_x$  thermoelectrics", *Phys. Chem. Chem. Phys.*, **18**(2), 939-946. <https://doi.org/10.1039/C5CP06163F>
- Kitagawa, H., Kurata, A., Araki, H., Morito, S. and Tanabe, E. (2010), "Effect of Deformation Temperature on Texture and Thermoelectric Properties of  $Bi_{0.5}Sb_{1.5}Te_3$  Prepared by Hot-Press Deformation", *J. Electron.*

- Mater.*, **39**, 1692-1695. <https://doi.org/10.1007/s11664-010-1181-9>
- Lee, D.M., Lim, C.H., Cho, D.C., Lee, Y.S. and Lee, C.H. (2006), "Effects of annealing on the thermoelectric and microstructural properties of deformed n-type Bi<sub>2</sub>Te<sub>3</sub>-based compounds", *J. Electron. Mater.*, **35**, 360-365. <https://doi.org/10.1007/BF02692457>
- Lee, D.H., Lee, J.U., Jung, S.J., Baek, S.H., Kim, J.H., Kim, D.I., Hyun, D.B. and Kim, J.S. (2014), "Effect of heat treatment on the thermoelectric properties of Bismuth–Antimony–Telluride prepared by mechanical deformation and mechanical alloying", *J. Electron. Mater.*, **43**, 2255-2261. <https://doi.org/10.1007/s11664-014-3037-1>
- Liu, H., Chen, Y., Tang, Y., Wei, S. and Niu, G. (2007), "The microstructure, tensile properties and creep behaviour of as-cast Mg-(1-10) %Sn alloys", *J. Alloys Compd.*, **440**(1-2), 122-126. <https://doi.org/10.1016/j.jallcom.2006.09.024>
- Lu, H., Wang, C.A., Huang, Y. and Xie, H. (2014), "Multi-Enhanced-Phonon Scattering Modes in Ln-Me-A Sites co-substituted LnMeA11O19 Ceramics", *Sci. Rep.*, **4**, 6823. <https://doi.org/10.1038/srep06823>
- Macario, L.R., Cheng, X., Ramirez, D., Mori, T. and Kleinke, H. (2018), "Thermoelectric properties of Bi-doped magnesium silicide stannides", *ACS Appl. Mater. Inter.*, **10**(47), 40585-40591. <https://doi.org/10.1021/acsami.8b15111>
- Mark, B. (2013), "Remarkable magnesium: the 21<sup>st</sup> century structural alloy for small components", FisherCast Global Corporation.
- Mezbahul-Islam, M., Mostafa, A.O. and Medraj, M. (2014), "Essential magnesium alloys binary phase diagrams and their thermochemical data", *J. Mater.*, **2014**, 1-33. <https://doi.org/10.1155/2014/704283>
- Minnich, A.J., Dresselhaus, M.S., Ren, Z.F. and Chen, G. (2009), "Bulk nanostructured thermoelectric materials: current research and future prospects", *Energy Environ. Sci.*, **2**(5), 466-479. <https://doi.org/10.1039/B822664B>
- Ray, R.K. and Jonas, J.J. (1990), "Transformation textures in steels", *Int. Mater. Rev.* **35**(1), 1-36. <https://doi.org/10.1179/095066090790324046>
- Rowe, D.M. (1995), *CRC Handbook of Thermoelectrics*, CRC Press, Boca Raton, Florida, United States.
- Sahoo, S.K., Sabat, R.K., Panda, S., Mishra, S.C. and Suwas S. (2015), "Mechanical property of pure magnesium: from orientation perspective pertaining to deviation from basal orientation", *J. Mater. Eng. Perf.*, **24**(6), 2346-2353. <https://doi.org/10.1007/s11665-015-1522-1>
- Santos, R., Yamini, S.A. and Dou, S.X. (2018), "Recent progress in magnesium-based thermoelectric materials", *J. Mater. Chem. A*, **6**(8), 3328-3341. <https://doi.org/10.1039/C7TA10415D>
- Shakouri, A. (2011), "Recent developments in semiconductor thermoelectric physics and materials", *Annu. Rev. Mater. Res.*, **41**, 399-431. <https://doi.org/10.1146/annurev-matsci-062910-100445>
- Snyder, G.J. and Toberer, E.S. (2008), "Complex thermoelectric materials", *Nat. Mater.*, **7**, 101-110. [https://doi.org/10.1142/9789814317665\\_0016](https://doi.org/10.1142/9789814317665_0016)
- Thiagarajan, S.J., Wang, W. and Yang, R. (2010), "Nanocomposites as high efficiency thermo- electric materials", *Annual Review of Nano Research*. World Scientific, Boulder, CO, USA.
- Tritt, T.M. (2002), "Thermoelectric Materials: Principles, Structure, Properties, and Applications", In: *Encyclopedia of Materials: Science and Technology*, Elsevier Science Ltd., 1-11.
- Tritt, T.M. (2004), *Thermal conductivity theory, properties, and applications*, Springer, New York, USA.
- Tritt, T.M. and Subramanian, M.A. (2006), "Thermoelectric materials, phenomena, and applications: a bird's eye view", *MRS Bull.*, **31**(3), 188-229. <https://doi.org/10.1557/mrs2006.44>
- Viennois, R., Colinet, C., Jund, P. and Tedenac, J.C. (2012), "Phase stability of ternary antiferrotype type compounds in the quasi binary systems Mg<sub>2</sub>X-Mg<sub>2</sub>Y (X, Y = Si, Ge, Sn) via ab-initio calculations", *Intermetallics*, **12**, 145-151. <https://doi.org/10.1016/j.intermet.2012.06.016>
- Wang, S., Yang, J., Toll, T., Yang, J., Zhang, W. and Tang, X. (2015), "Conductivity-limiting bipolar thermal conductivity in semiconductors", *Sci. Rep.*, **5**, 10136. <https://doi.org/10.1038/srep10136>
- Xu, Z.J., Hu, L.P., Ying, P.J., Zhao, X.B. and Zhu, T.J. (2015), "Enhanced thermoelectric and mechanical properties of zone melted p-type (Bi,Sb)<sub>2</sub>Te<sub>3</sub> thermoelectric materials by hot deformation", *Acta Mater.*, **84**, 385-392. <https://doi.org/10.1016/j.actamat.2014.10.062>

Zheng, J.C. (2008), "Recent advances on thermoelectric materials", *Front. Phys. China*, **3**, 269-279.  
<https://doi.org/10.1007/s11467-008-0028-9>

CC